Four-dimensional flow MRI using spiral acquisition

Andreas Sigfridsson, Sven Petersson, Carljohan Carlhäll and Tino Ebbers

4D flow MRI using spiral acquisition

Andreas Sigfridsson[1,2], Sven Petersson[1,2], Carl-Johan Carlhäll[2,3], Tino Ebbers[1,2,4]

1 Division of Cardiovascular Medicine, Department of Medical and Health Sciences, Linköping University, Linköping, Sweden.
2 Center for Medical Image Science and Visualization (CMIV), Linköping University, Linköping, Sweden.
3 Department of Clinical Physiology, Linköping University Hospital, Linköping, Sweden.
4 Division of Applied Thermodynamics and Fluid Mechanics, Department of Management and Engineering, Linköping University, Linköping, Sweden.

Running head: 4D flow MRI using spiral acquisition
Word count: 4105

Correspondence to
Andreas Sigfridsson,
KVM, Department of Medical and Health Sciences,
Linköping University,
SE-581 83 Linköping,
Sweden.
E-mail: andreas.sigfridsson@liu.se

Abstract

Time-resolved three-dimensional phase contrast MRI is an important tool for physiological as well as clinical studies of flow in the heart and vessels. The application of the technique is, however, limited by the long scan times required. In the present work, we investigate the feasibility of using spiral readouts to reduce the scan time of 4D flow MRI without sacrificing quality. Three spiral approaches are presented and evaluated *in-vivo* and *in-vitro* against a conventional Cartesian acquisition. *In-vivo*, the performance of each method was assessed in the thoracic aorta in ten volunteers using pathline based analysis and cardiac output analysis. SNR and background phase errors were investigated *in-vitro*.

Using spiral readouts, the scan times of a 4D flow acquisition of the thoracic aorta could be reduced two to threefold, with no statistically significant difference in pathline validity or cardiac output. The shortened scan time improves the applicability of 4D flow MRI, which may allow the technique to become a part of a clinical workflow for cardiovascular functional imaging.

Keywords: cine 3D flow, phase contrast, spiral, pathline

Grant support: Swedish Research Council, Swedish Heart-Lung Foundation

Introduction

Time resolved three-dimensional three-directional phase contrast MRI (4D flow) (1-4) is becoming an important tool for studies of the blood flow in the cardiovascular system. The technique has added to the understanding of the physiology and pathophysiology of the heart and great vessels (5-11), and has been shown to be valuable in various clinical applications (12-15).

The major limitation of existing implementations, however, is the excessively long scan time, currently in tens of minutes, which hinders application of the method in many cases, particularly in the clinical realm. The long scan times can be attributed to several factors: the high number of sampling points required to achieve the desired spatiotemporal resolution and coverage; the fourfold acquisition necessary to encode three velocity components; and the time necessary for applying the bipolar gradients. When imaging in the chest and abdomen, scan time is further increased by the use of respiratory gating, which reduces the time available for actual data sampling.

Techniques to reduce the acquisition time are available, but have all major drawbacks and involve reduced signal-to-noise ratio (SNR). It is possible to reduce the number of sampling points to decrease the acquisition time, but this may result in signal aliasing. With Cartesian sampling, the number of samples in the phase-encoding direction may be reduced to decrease the imaging time, but this results in fold-over artifacts in the phase-encoding direction which may be tolerable as long as they occur outside of the heart or vessels. With non-Cartesian sampling, the aliasing artifacts will be less structured. The aliasing artifacts in, for example, a spiral acquisition will be spread in all directions (the two in-plane directions in the case of a stack of spirals) and over the whole field of view. The use of a variable-density spiral trajectory, with higher sampling density at the center of k-space, may reduce these artifacts (16). Several different techniques can be used to decrease the number of sampling points while avoiding aliasing artifacts. A commonly applied technique is parallel imaging

(17-18), where the coil sensitivity variations of multiple coil elements can be used to reconstruct the data from fewer samples without aliasing artifacts. Sparsity in the spatio-temporal reciprocal of the sampling domain can also be used to reduce the number of samples needed (19-21). Parallel imaging and *k*-*t* SENSE have been used previously to reduce scan times for phase-contrast MRI using Cartesian approaches (22-23). However, sufficient reduction factors for parallel imaging have not been reached, and some temporal smoothing remains for *k*-*t* SENSE approaches. Constraining the reconstruction problem using principal component analysis (24) seems promising to reduce the scan time for 4D flow (25), while it has not yet been demonstrated for cardiac flow imaging.

The scan time can also be reduced by sampling with a higher bandwidth, i.e. by traversing the *k*-space more quickly (26). Due to the time required for excitation and velocity encoding using the bipolar gradients, a higher bandwidth is not cost-effective in conventional spin-warp (non-echo-planar) or radial imaging. It can be very beneficial in echo-planar imaging or spiral acquisition, however, especially when combined with an extended readout duration to cover more of *k*-space (27, 3, 28). Radial sampling allows for high efficiency in this manner, which can be used to improve spatial resolution rather than reduce scantime (29-30). Reductions in scan time can only be obtained in combination with undersampling, which in practice becomes a necessity since radial sampling fulfilling Nyquist criterion requires a factor of pi/2 readouts compared to Cartesian sampling. Spiral acquisition should be more appropriate when aiming for short scan times rather than high spatial resolution, and the high efficiency of spiral readouts has previously been exploited for two-dimensional flow imaging in breath hold and real time imaging (31-33). In addition to the decrease in scan time, spiral acquisition also offers some inherent insensitivity to flow induced errors. However, spiral readouts have also failed to gain clinical acceptance due to decreased robustness to system imperfections and sensitivity to off-resonance. In the light of recent advances in hardware and computational algorithms, these effects may be corrected for. Off-resonance and susceptibility effects can also be limited by keeping the readout durations sufficiently short.

In the present work, we investigate the feasibility of using spiral readouts to reduce the scan time of 4D flow MRI without sacrificing quality. We present and evaluate three acquisition approaches using stack of spiral readouts . The spiral acquisitions are evaluated in-vivo against a conventional Cartesian acquisition with identical spatiotemporal resolution using pathline analysis and computation of cardiac output. Additionally, SNR and background phase errors are investigated in-vitro.

Methods

A time resolved three-dimensional three-directional velocity imaging pulse sequence using spiral readouts was implemented on a clinical 1.5T MRI system. The performance of this pulse sequence was validated against a conventional Cartesian acquisition with identical spatiotemporal resolution. The acquisitions were compared using pathline analysis and volume flow. Pathlines accumulate any errors in the velocity field along the trace and spatiotemporal fidelity is then assessed as the conformance of the pathlines with the geometrical constraints of the vessels. In addition, cardiac output measures from the three-dimensional acquisitions were compared with those from a two-dimensional (2D) through-plane velocity measurement. In-vitro measurements on a stationary phantom were performed in order to investigate the SNR and background phase errors of the different acquisitions.

Acquisition

A clinical 1.5 T MRI system (Achieva, Philips, Best, The Netherlands) with 33mT/m gradient strength and 180 T/m/s slew rate and a 5 element cardiac SENSE coil was used for signal reception for all acquisitions. Interleaved stack-of-spiral trajectories were used to traverse a three-dimensional *k*-space after

volumetric slab excitation and bipolar gradient waveforms for flow sensitivity, as illustrated in Figure 1.

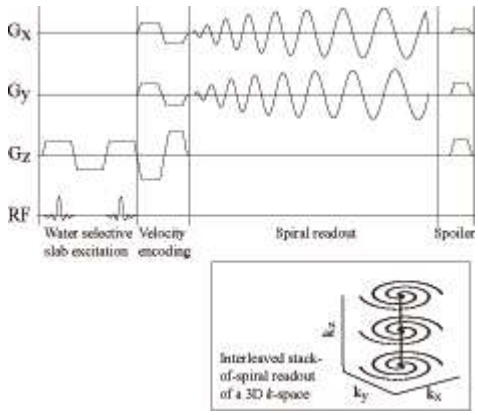

Figure 1. Pulse sequence diagram showing a pulse sequence schematic for the spiral acquisition. After a 1-1 water-selective spectral-spatial slab excitation pulse and bipolar velocity encoding, spiral readouts are used to acquire data. With this pulse sequence, a temporally resolved 3D *k*-space is sampled one spiral arm at a time, as shown in the schematic below.

Spiral acquisition is hampered by signal from fat, which is off-resonance and causes blurring in the image. In order to suppress fat induced signal, a spatial-spatial excitation was used in the spiral acquisition (34). Because of the need for a short TR, a 1-1 spectral-spatial pulse was used. In pilot experiments, the use of 1-1 spectral-spatial water excitation pulses showed significantly improved visual image quality, while a 1-2-1 scheme was determined not to justify the longer pulse duration.

In Cartesian phase contrast imaging, the four velocity encoded scan segments of a single line in *k*-space are often acquired in succession within the same heart phase. Additionally, short TR pulse sequences allow for more than one *k*-space line to be acquired per cardiac cycle and still maintain a reasonable temporal resolution. In this study, we used a Cartesian TR of 6.1 ms and acquired 2 *k*-space lines per cardiac cycle, achieving a nominal temporal resolution of 48.8 ms (2x4xTR), similar to previous studies (8). In spiral imaging, other design choices with respect to the acquisition order are available. In this study, three different spiral configurations were tested. All of them extend the TR to improve efficiency by using a longer readout and covering more of *k*-space after the spectral-spatial

excitation and bipolar gradients. The first configuration, referred to as TR-interleaved, acquires one spiral interleave per cardiac cycle and interleaves the velocity scan segments every TR within one heart phase. The resulting nominal temporal resolution is 1x4xTR, so that a chosen TR of 12.2 ms resulted in the same temporal resolution of 48.8 ms. The second configuration, referred to as beat-interleaved, aims to extend the efficiency further by interleaving the velocity encoded scan segments on a per beat basis. By acquiring three spiral interleaves per beat, the nominal temporal resolution is 3x1xTR, resulting in a TR of 16.3 ms. The total number of interleaves were chosen so that the beat-interleaved acquisition had the same total scan time as the TR-interleaved acquisition. A third configuration, referred to as "short beat-interleaved" pushes the limits further by reducing the total number of interleaves, but is otherwise identical to the beat-interleaved acquisition. The temporal resolution, i.e. the duration between two successive samples of every *k*-space location, is identical for all acquisitions, and no temporal smoothing was performed in reconstruction. The acquisition order is illustrated in Figure 2.

Ten healthy volunteers (nine men and one woman, age 31±6 years, heart rate 64±13 beats per minute) were imaged after approval by the regional ethics committee and with written consent from all participants. The participants were instructed to lie as still as possible in the scanner and breathe slowly. An imaging slab of 45-50 mm thickness was placed to cover the thoracic aorta, and the four different flow acquisitions were performed in randomized order. Additionally, a standard two-dimensional through-plane flow measurement was applied in the proximal ascending aorta (parameters according to the local clinical protocol used: TE 2.6 ms, TR 4.8 ms, matrix 128x98, FOV 320x260 mm, voxel size 2.5x2.7 mm, slice thickness 8 mm, SENSE reduction factor 2.0, VENC 200 cm/s, flip angle 12°, 4 *k*-space lines per cardiac cycle).

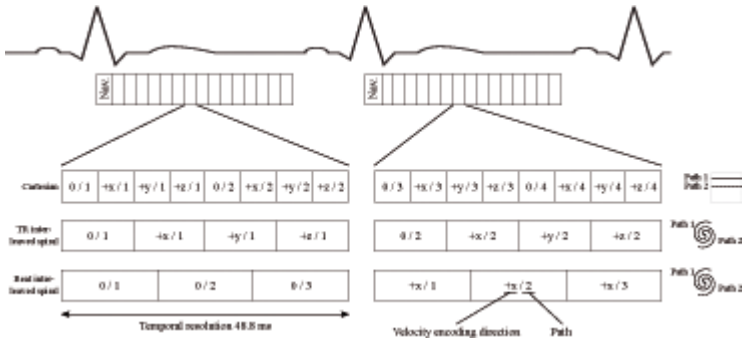

Figure 2. Acquisition order for the different velocity encoding segments and paths read out for the different pulse sequences. Both the beat-interleaved spiral and the short beat-interleaved spiral share the same acquisition order. The Cartesian acquisition reads all four velocity encodings of two lines in *k*-space per heart phase and beat. The TR-interleaved spiral reads all four velocity encodings for a single spiral interleave per heart phase and beat. The beat-interleaved spiral acquisitions read out a single velocity encoded segment of three spiral interleaves per heart phase and beat. The temporal resolution, i.e. the duration between successive sampling of *k*-space locations, for all methods is identical (48.8 ms) and no temporal smoothing is performed in reconstruction.

The pulse sequence parameters for all 4D pulse sequences are listed in Table 1. Prospective cardiac gating was used, a respiratory navigator with a gating window of 5 mm was used to shift the acquisition volume according to the respiratory motion (tracking). Volume shim was used with a shim box covering the aortic arch and the descending aorta. The flip angle was chosen as the Ernst angle in order to achieve the highest constant SNR for a steady-state acquisition. The in-plane field of view for the spiral acquisitions were set to 260 mm, as pilot tests indicated that using this would be possible to reach substantial time savings without compromising the image quality significantly, likely due to the limited coil sensitivity of the five-channel SENSE coil used. The total time for each volunteer in the scanner was approximately one hour.

During data reconstruction, effects of concomitant gradients (Maxwell terms) were automatically corrected (35). In post-processing, background phase offsets were subtracted using a second order polynomial fitting to static tissue detected using temporal variance (36). After this step, the phase was unwrapped by removing pairs of phase jumps in the temporal dimension.

In-vitro measurements were performed on a stationary phantom in order to compare the background phase errors and SNR of the four different measurements. The same pulse sequences as used in the in-vivo measurements were used, with exception of that only a single timeframe was collected and no respiratory and cardiac gating was used. Furthermore, for each acquisition an additional noise reference measurement, in which all gradients and RF pulses were turned off, was performed.

Analysis

The quality of the *in-vivo* data of the spiral acquisitions was evaluated by comparison of the data from the Cartesian acquisition, as phantom studies are unable to reflect realistic *in-vivo* conditions such as flow patterns , respiratory motion, cardiac motion, and off-resonance effects . 4D flow MRI acquisitions are primarily evaluated using volume flow and pathline analysis. Pathline analysis demands high quality velocity data, as any errors including noise in the velocity data are accumulated during the course of trajectory integration. The spatiotemporal fidelity and accuracy of the velocity field is thus reflected in the validity of the trajectories. Therefore, we evaluated spiral acquisitions by comparison to the well-established standard Cartesian acquisition using a data-driven approach in which pathlines, particle traces integrated over time, were used to analyze the quality of the velocity data sets. Accurate pathlines should never leave the blood pool. Although pathlines that do not leave the bloodpool are not necessarily accurate, the number of traces that are not contained within the geometrical boundaries of the aortic wall reflect the quality of the data.

For each acquisition, the aorta was segmented based on the complex-difference phase contrast angiogram derived from the flow data itself. The signal level in these data reflects both signal magnitude and flow presence. To obtain a binary mask for the aorta, thresholding was used. The thresholds were set to obtain identical volumes for a section of the aorta determined by anatomical landmarks for all four acquisitions for each subject. The inlet landmark was defined as the ascending aorta at the level of the pulmonary artery. The outlet landmark was defined as the descending aorta at the inferior level of the left atrium. The supra-

aortic branches were excluded from the segmentation. The section of the aorta studied is illustrated in Figure 3. The volumes of the segmentations averaged 87.5±6.3 ml.

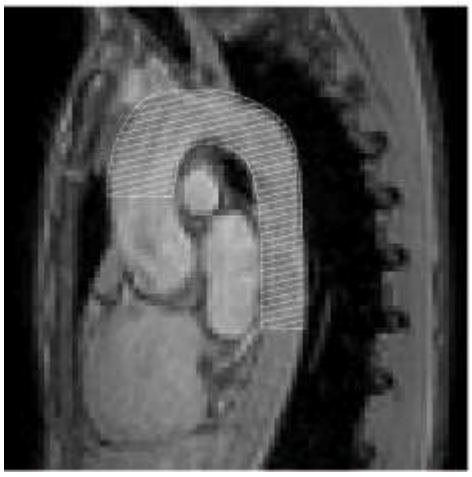

Figure 3. Schematic drawing of the segment of the thoracic aorta studied. The aortic segmentation starts at the level of the pulmonary artery in the ascending aorta and stops at the inferior limit of the left atrium. The supra-aortic branches are removed from the segmentation. The threshold of the angiogram used is chosen so as to achieve identical volumes for all four acquisitions of each volunteer.

The number of traces that stayed within the segmentation border determined the quality of each acquisition. In order to avoid the difficulty of distinguishing pathlines appropriately leaving the aorta through branching arteries from pathlines leaving the segmentation due to data quality issues, backward pathlines were used. The traces were emitted from the descending aorta at the inferior level of the left atrium. The emission time was set to the downslope of the volume flow curve at the site of emission, for each subject individually. The emission duration encompassed all data acquired back to the first time frame. Traces reaching the ascending aorta at the level of the pulmonary artery were not counted as having left the segmentation. Additionally, in order to evaluate the performance in a low velocity setting, diastolic flow was also analyzed. Traces were released from the entire segmented volume during the four last time frames in the forward direction, and the number of traces that remained within the segmentation was computed.

Pathlines, particle traces integrated over time, were computed by custom software using a four-stage Runge-Kutta integration scheme with quad-linear spatiotemporal interpolation, as suggested in the literature (37). The step length was set to 5 ms, which was determined in a pilot test to be sufficiently short given the temporal resolution. For one example visualization figure, streamlines were also generated using the same software and settings, although without stepping forward in time during the course of the integration.

Two independent observers inspected the pathlines of each dataset visually, looking for apparent differences between the methods with respect to abrupt flow trajectories, non-physiological flow and general appearance of flow patterns.

Further evaluation of the data quality was obtained by comparison of the axial through plane flow in the ascending aorta with a two-dimensional breath held acquisition. The three-dimensional images were reformatted to the same slice location and orientation using cubic interpolation based on the image coordinates in the reconstructed DICOM images. The reformatted images were then segmented using Segment v1.8 R1189 (38) using two observers. The cardiac output in the ascending aorta was computed for each acquisition and compared. The average result from the two observers is reported in the results section.

For the in-vitro measurement, both the magnitude and the noise data were reconstructed without compensating for coil sensitivity and divided by the SENSE g-factor map to obtain spatially uniform noise (39-40). In order to obtain the SNR in all voxels, the signal magnitude was divided by the standard deviation of the noise data. The mean and standard deviation of the SNR in a segmentation of the phantom were then computed for all four measurements. The background phase errors were measured over a region of interest in the phantom both before and after phase correction.

Statistical analysis

Group mean values are reported as mean ± 1 SD. Level of significance was set to $p<0.05$ unless otherwise stated. Both pathlines and 2D volume flow were analyzed using a two-way ANOVA with Tukey post-hoc test for multiple comparisons using Minitab version 16.1.1.0. Inter-observer comparison for cardiac output was performed using paired t-test, level of significance was adjusted to $p<0.05/5$ after Bonferroni-correction. Additionally, a Bland-Altman analysis was performed on the cardiac output values.

Results

All acquisitions and reconstructions were completed successfully. The actual scan times are listed in Table 2. The average navigator gating efficiency was 64 ±10 %.

Visual inspection of the particle traces did not reveal any artifacts or other discrepancies (see figures 4 and 5). No apparent differences could be seen between the four different acquisitions by the two observers. The majority of the particle traces resembled physiologically reasonable paths for all acquisitions, and the backwards pathlines reached the aortic valve plane in all acquisitions. Quantitative assessment of the quality of the data sets, reflected by the number of traces that remain within the segmentation, is shown for the four different acquisitions in Table 3. There were no statistically significant differences between any acquisition methods for the systolic traces. For the diastolic traces, the number of traces within the segmentation was higher for the Cartesian and TR interleaved spiral methods, compared to the beat and short beat interleaved methods.

An estimate for the cardiac output was computed for the 4D acquisitions as well as for the through-plane acquisition, and the results are shown in Table 4. There were no statistically significant differences between the cardiac output estimates from the two observers except for the through-plane measurement, where there

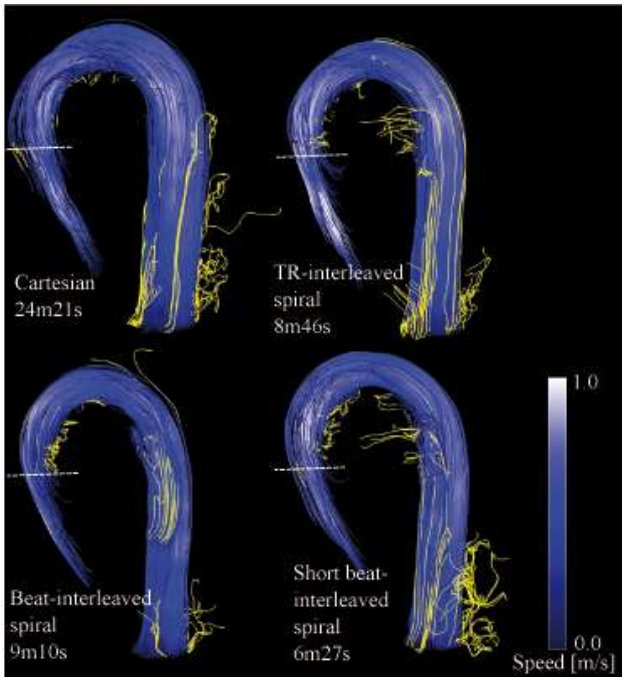

Figure 4. Pathlines for all four 4D flow acquisitions from a single volunteer. Pathlines were traced backwards from the descending aorta to avoid branching flow. Traces remaining within the aortic segmentation are colored according to speed, but are colored yellow where the traces exit the segmentation. Traces reaching level of the pulmonary artery, indicated by the dotted line, were not counted as leaving the segmentation.

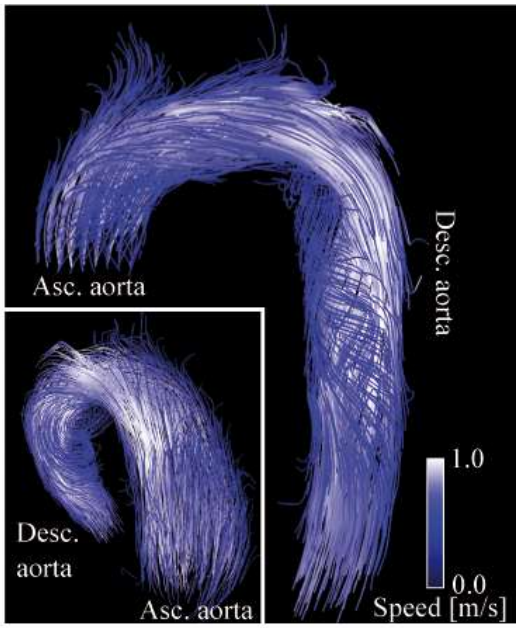

Figure 5. Forward streamlines emitted in late systole from the entire aortic mask from the short beat-interleaved spiral acquisition of a healthy volunteer (acquisition time 2m39s). The helical flow in the ascending as well as the descending aorta was well depicted in all four acquisitions of this volunteer.

was a mean difference of 0.28±0.26 l/min ($p<0.008$) between the two readers. There were statistically significant differences between the through-plane measurement and the two beat-interleaved spiral acquisitions, however no statistically significant difference was found between any of the 4D acquisitions, including Cartesian. A Bland-Altman plot is shown in Figure 6. The biases were lowest for the Cartesian, TR-interleaved and beat-interleaved spiral acquisition, and highest for the through-plane acquisition. The limits of agreement were similar for all 3D methods but higher for the through-plane acquisition.

The background phase errors in the in-vitro measurements are shown in Table 5. Before phase correction, the phase errors in the spiral acquisitions are higher compared to the Cartesian acquisition, but after correction the phase errors are similar for all methods. The results from the in-vitro SNR measurement are presented in Table 6. The SNR for all methods is comparable, but the beat-interleaved spiral acquisition had the highest mean SNR.

Discussion

A time resolved three-dimensional three-directional velocity imaging (4D flow) pulse sequence using spiral readouts was implemented and validated in the normal thoracic aorta against a conventional Cartesian acquisition. Compared to a conventional Cartesian acquisition, up to a threefold decrease in scan time was achieved without a noticeable decrease in flow data quality for the systolic pathlines. For the diastolic pathlines, slightly reduced flow data quality was observed for the two beat-interleaved spiral acquisitions, but the TR-interleaved spiral acquisition, which provides a twofold decrease in scan time, had no difference in flow data quality compared to the Cartesian acquisition. All methods compared had similar SNR, but the beat-interleaved spiral acquisition provided slightly higher SNR. Background phase errors were higher in the spiral acquisitions, but could be corrected successfully for all methods. Cardiac output estimated from a through-plane acquisition was significantly higher than two of the spiral acquisitions, but there was no statistically significant difference between the Cartesian and spiral three-dimensional acquisitions or between the

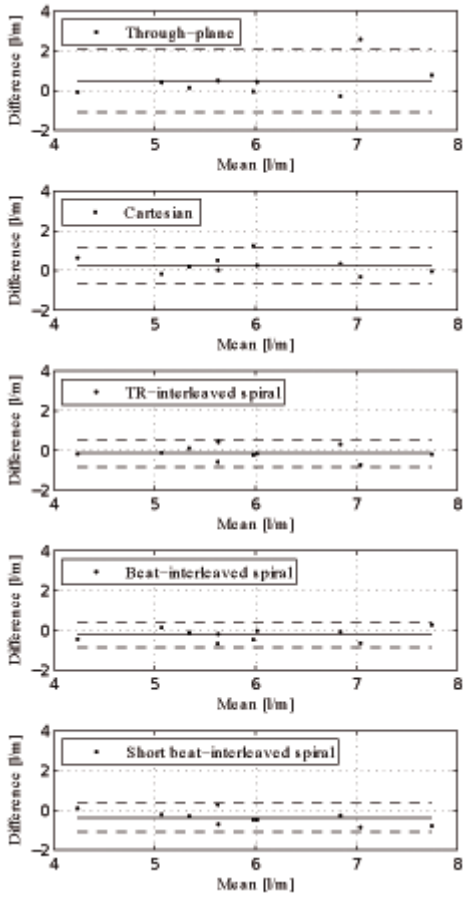

Figure 6. Bland-Altman plot of the cardiac output measures from all methods. The difference between each method and their mean (of the five methods) are plotted against the mean on the horizontal axis. The biases are indicated with solid line and the limits of agreement are indicated with dashed lines.

through-plane acquisition and the TR-interleaved spiral or the Cartesian acquisitions. The through-plane acquisition had highest bias and widest level of agreement in a Bland-Altman analysis, but the Cartesian and spiral acquisitions were similar to each other.

The pathline based analysis provides a data consistency measure by integrating the velocity field over space and time and comparing to the geometrical constrains of the vessel lumen. The fraction of traces that stayed within the segmentation was similar to what has been reported previously in the literature (41). Using this analysis, no significant differences could be found between the spiral and Cartesian acquisitions for systolic pathlines. There was a trend towards higher data consistency with the TR interleaved spiral acquisition compared to the Cartesian acquisition, possibly due to advantageous effects

related to the shorter scan time. The shorter scan time results in smaller changes in respiratory patterns and heart rate during the scan, and reduces the risk for patient movement. For the diastolic pathlines, the two beat-interleaved acquisitions had lower data consistency compared to TR-interleaved spiral and Cartesian acquisitions. This might be related to the timing effects of the beat-interleaved scheme.

Volume flow was also assessed with the different methods. The 2D through-plane acquisition yielded the highest cardiac outputs on average. This is not surprising given the significantly higher temporal resolution and whole cardiac cycle coverage of the retrospectively gated 2D method. While the 2D through-plane method provided statistically significantly higher cardiac outputs than the two beat-interleaved spiral acquisitions, no statistically significant difference could be detected in comparison with the Cartesian acquisition or the TR-interleaved spiral acquisition. Comparing the Cartesian and spiral 4D acquisitions to each other, no statistically significant differences could be found. Spiral acquisitions may provide the short acquisition time required to replace multiple through-plane acquisitions with a single 4D acquisition, however, higher temporal resolution would likely be required to provide more accurate measures of cardiac output. In this study, we used the same temporal resolution in all spiral as well as Cartesian acquisitions. This temporal resolution was mainly defined by the scan time of the Cartesian acquisition. Spiral acquisitions can be performed with better temporal resolution, however, further studies are required to validate spiral acquisition approaches with higher temporal resolution in order to determine if the accuracy of the 4D volume flow measurements can be improved sufficiently.

The background phase errors in the spiral methods were higher compared to the Cartesian acquisition, when no correction was performed. This is likely due to short-term eddy current effects in the center of *k*-space, which is read out directly after the bipolar gradient in the spiral acquisitions. However, after the phase correction was applied, the remaining phase errors were similar for all methods.

The on-line reconstruction did not support correction for blurring caused by off-resonance during spiral readouts. Nevertheless, in this work, the imaged field of view allowed for a targeted shim volume to reach an off-resonance of ±32 Hz in the aortic segmentation as estimated from the phase of the flow-nulled segment. In combination with the short spiral readouts used, this corresponds to a point-spread-function with a full-width-half-maximum of 1.3 pixels or better, even without off-resonance correction. For larger field of views and higher spatial resolution, or when using higher field strengths, reconstruction techniques robust to off-resonance should be considered (42). Additionally, effects of blurring caused by off-resonance may need to be further investigated in the setting of flow quantification.

The study was performed using *prospective* cardiac gating, a technique commonly used for 4D flow MRI of vessels. For studies where it is important to cover the entire cardiac cycle e.g. intracardiac flow, *retrospective* gating is required to depict the complete diastolic flow. The use of retrospective gating may also have advantages related to the different orderings of the acquisitions (as shown in Figure 2). In particular, early systolic flow, directly after the ECG trigger, can be easily missed with the later acquisition of the center of *k*-space in the prospectively gated spiral acquisitions. With retrospective cardiac gating, this will not result in any data loss, as the complete cardiac cycle is covered.

Cartesian acquisition is a mature technique that has been studied and used extensively in the past. While there is also a large experience with spiral acquisition, new improvements or even pitfalls may remain to be found in its use for 4D flow imaging and is a field where more research is necessary. Parallel imaging could be used to further reduce the scan time of spiral imaging. However, in-plane parallel imaging was not available for the spiral acquisitions in this study. Parallel imaging in the slice direction was available, but was not used in this study due to the relatively thin slab thickness, which would result in very small variation of coil sensitivity across the slab. In-plane parallel imaging could be more efficient in this case, depending on the slab orientation and coil

element layout, although it may require longer reconstruction times (43). Parallel imaging using GRAPPA (44) may be more suitable for spiral imaging. The scan time reductions achieved by using the spiral readout in this work is a factor of two to three, despite the absence of parallel imaging as compared to the Cartesian approach compared with. Despite the reduction of scan time, the SNR of all methods are comparable. Parallel imaging can be used to further reduce scan time, but the impact of the SNR penalty associated with parallel imaging needs to be evaluated. Further improvements to the spiral acquisition include measuring the actual gradient waveforms and compensating for deviations from the spiral pattern (45). An alternative to stack-of-spirals is to rotate the spirals, covering an isotropic 3D *k*-space (46).

In conclusion, using spiral acquisition, the scan time of 4D flow MRI acquisitions can be reduced two- to threefold compared to conventional Cartesian acquisition without reducing the data quality for pathline analysis and measurement of cardiac output. This may open the door to large research studies and clinical use of 4D flow MRI, whose use to this point has been hampered by excessively long scan times.

References

1. Firmin D, Gatehouse P, Konrad J, Yang G, Kilner P, Longmore D. Rapid 7-dimensional imaging of pulsatile flow. In Proc Comput Cardiol. 1993; 353-356.
2. Wigström L, Sjöqvist L, Wranne B. Temporally resolved 3D phase-contrast imaging. Magn Reson Med 1996;36(5):800-803.
3. Kozerke S, Hasenkam J, Pedersen E, Boesiger P. Visualization of flow patterns distal to aortic valve prostheses in humans using a fast approach for cine 3D velocity mapping. J Magn Reson Imaging 2001;13(5):690-698.
4. Markl M, Chan F, Alley M, Wedding K, Draney M, Elkins C, Parker D, Wicker R, Taylor C, Herfkens R, et al. Time-resolved three-dimensional phase-contrast MRI. J Magn Reson Imaging 2003;17(4):499-506.
5. Kilner P, Yang G, Wilkes A, Mohiaddin R, Firmin D, Yacoub M. Asymmetric redirection of flow through the heart. Nature 2000;404(6779):759-761.
6. Hope T, Herfkens R. Imaging of the Thoracic Aorta with Time-Resolved Three-Dimensional Phase-Contrast MRI: A Review. Sem Thoracic and Cardiovasc Surg 2008;20:358-364.
7. Dyverfeldt P, Kvitting J, Sigfridsson A, Engvall J, Bolger A, Ebbers T. Assessment of fluctuating velocities in disturbed cardiovascular blood flow: In vivo feasibility of generalized phase-contrast MRI. J Magn Reson Imaging 2008;28(3):655-663.
8. Eriksson J, Dyverfeldt P, Engvall J, Bolger AF, Ebbers T, Carlhall CJ. Quantification of Pre-systolic Blood Flow Organization and Energetics in the Human Left Ventricle. Am J Physiol Heart Circ Physiol. 2011;300:H2135-2141.
9. Carlhäll CJ, Bolger A. Passing Strange: Flow in the Failing Ventricle. Circ Heart Fail 2010;3(2):326.
10. Markl M, Kilner P, Ebbers T. Comprehensive 4D velocity mapping of the heart and great vessels by cardiovascular magnetic resonance. J Cardiovasc Magn Reson 2011;13(1):7.
11. Ebbers T. Flow Imaging: Cardiac Applications of 3D Cine Phase-Contrast MRI. Curr Cardiovasc Imaging Rep 2011;4:127–133.
12. Roes SD, Hammer S, van der Geest RJ, et al. Flow assessment through four heart valves simultaneously using 3-dimensional 3-directional velocity-encoded magnetic resonance imaging with retrospective valve tracking in healthy

volunteers and patients with valvular regurgitation. Invest Radiol 2009;44:669–675.
13. Harloff A, Simon J, Brendecke S, Assefa D, Helbing T, Frydrychowicz A, Weber J, Olschewski M, Strecker C, Hennig J, et al. Complex Plaques in the Proximal Descending Aorta: An Underestimated Embolic Source of Stroke. Stroke 2010;41(6):1145.
14. Hope M, Meadows A, Hope T, Ordovas K, Saloner D, Reddy G, Alley M, Higgins CB. Clinical Evaluation of Aortic Coarctation With 4D Flow MR Imaging. J Magn Reson Imaging 2010;31:711–718.
15. Markl M, Geiger J, Kilner P, Föll D, Stiller B, Beyersdorf F, Arnold R, Frydrychowicz A. Time-resolved three-dimensional magnetic resonance velocity mapping of cardiovascular flow paths in volunteers and patients with Fontan circulation. Eur J Cardiothorac Surg 2011;39:206-212.
16. Tsai CM, Nishimura DG. Reduced aliasing artifacts using variable-density *k*-space sampling trajectories. Magn Reson Med 2000;43:452-458
17. Pruessmann K, Weiger M, Scheidegger M, Boesiger P. SENSE: sensitivity encoding for fast MRI. Magn Reson Med 1999;42(5):952-962.
18. Griswold M, Jakob P, Heidemann R, Nittka M, Jellus V, Wang J, Kiefer B, Haase A. Generalized autocalibrating partially parallel acquisitions (GRAPPA). Magn Reson Med 2002;47(6):1202-1210.
19. Madore B, Glover G, Pelc N. Unaliasing by Fourier-encoding the overlaps using the temporal dimension (UNFOLD), applied to cardiac imaging and fMRI. Magn Reson Med 1999;42(5):813-828.
20. Tsao J, Boesiger P, Pruessmann K. k-t BLAST and k-t SENSE: Dynamic MRI with high frame rate exploiting spatiotemporal correlations. Magn Reson Med 2003;50(5):1031-1042.
21. Kellman P, Epstein F, McVeigh E. Adaptive sensitivity encoding incorporating temporal filtering (TSENSE). Magn Reson Med 2001;45(5):846-852.
22. Thunberg P, Karlsson M, Wigström L. Accuracy and reproducibility in phase contrast imaging using SENSE. Magn Reson Med 2003;50(5):1061-1068.
23. Baltes C, Kozerke S, Hansen M, Pruessmann K, Tsao J, Boesiger P. Accelerating cine phase-contrast flow measurements using k-t BLAST and k-t SENSE. Magn Reson Med 2005;54(6):1430-1438.

24. Pedersen H, Kozerke S, Ringgaard S, Nehrke K, Kim W. k-t PCA: Temporally constrained k-t BLAST reconstruction using principal component analysis. Magn Reson Med 2009;62(3):706-716.
25. Knobloch V, Giese D, Boesiger P, Kozerke S. Hadamard-Transform k-t PCA for Cine 3D Velocity Vector Field Mapping of Carotid Flow. In ISMRM. 2010; 67.
26. Bernstein MA, King KE, Zhou XJ. Handbook of MRI pulse sequences. Academic Press, 2004.
27. McKinnon G, Debatin J, Wetter D, von Schulthess G. Interleaved Echo Planar Flow Quantitation. Magn Reson Med 1994; 32:263-267.
28. Brix L, Ringgaard S, Rasmusson A, Sörensen T, Kim WY. Three dimensional three component whole heart cardiovascular magnetic resonance velocity mapping: comparison of flow measurements from 3D and 2D acquisitions. J Cardiovasc Magn Reson 2009;11:3
29. Gu T, Korosec F, Block W, Fain S, Turk Q, Lum D, Zhou Y, Grist T, Haughton V, Mistretta C. PC VIPR: a high-speed 3D phase-contrast method for flow quantification and high-resolution angiography. Am J Neuroradiol 2005;26(4):743.
30. Bieging E, Frydrychowicz A, Wentland A, Landgraf B, Johnson K, Wieben O, François C. In vivo three-dimensional MR wall shear stress estimation in ascending aortic dilatation. J Magn Reson Imaging 2011;33(3):589-597.
31. Gatehouse P, Firmin D, Collins S, Longmore D. Real time blood flow imaging by spiral scan phase velocity mapping. Magn Reson Med 1994;31(5):504-512.
32. Pike G, Meyer C, Brosnan T, Pelc N. Magnetic resonance velocity imaging using a fast spiral phase contrast sequence. Magn Reson Med 1994;32(4):476-483.
33. Nayak K, Pauly J, Kerr A, Hu B, Nishimura D. Real-time color flow MRI. Magn Reson Med 2000;43(2):251-258.
34. Meyer C, Pauly J, Macovskiand A, Nishimura D. Simultaneous spatial and spectral selective excitation. Magn Reson Med 1990;15(2):287-304.
35. Bernstein M, Zhou X, Polzin J, King K, Ganin A, Pelc N, Glover G. Concomitant gradient terms in phase contrast MR: analysis and correction. Magn Reson Med 1998;39(2):300-308.

36. Walker P, Cranney G, Scheidegger M, Waseleski G, Pohost G, Yoganathan A. Semiautomated method for noise reduction and background phase error correction in MR phase velocity data. J Magn Reson Imaging 1993;3(3):521-530.
37. Darmofal D, Haimes R. An analysis of 3D particle path integration algorithms. J Comput Phys 1996;123(1):182-195.
38. Heiberg E, Sjögren J, Ugander M, Carlsson M, Engblom H, Arheden H. Design and validation of Segment- freely available software for cardiovascular image analysis. BMC Medical Imaging 2010;10(1):1.
39. Kellman P, McVeigh E. Image reconstruction in SNR units: a general method for SNR measurement. Magn Reson Med 2005;54:1439–47.
40. Kellman P. Erratum to Kellman P, McVeigh ER. Image reconstruction in SNR units: a general method for SNR measurement. Magn Reson Med. 2005;54:1439-1447. Magn Reson Med 2007;58:211–2
41. Bock J, Frydrychowicz A, Stalder A, Bley T, Burkhardt H, Hennig J, Markl M. 3D Phase contrast MRA and flow visualization in the thoracic aorta at 3T: feasibility and effect of standard and blood-pool contrast agents. Magn Reson Med 2010;63:330-338.
42. Börnert P, Schomberg H, Aldefeld B, Groen J. Improvements in spiral MR imaging. MAGMA 1999;9:29–41.
43. Pruessmann K, Weiger M, Börnert P, Boesiger P. Advances in sensitivity encoding with arbitrary *k*-space trajectories. Magn Reson Med 2001;46(4):638-651.
44. Heidemann R, Griswold M, Seiberlich N, Krüger G, Kannengiesser S, Kiefer B, Wiggins G, Wald L, Jakob P. Direct parallel image reconstructions for spiral trajectories using GRAPPA. Magn Reson Med 2006;56(2):317-326.
45. Barmet C, Zanche N, Pruessmann K. Spatiotemporal magnetic field monitoring for MR. Magn Reson Med 2008;60(1):187-197.
46. Koladia KV, Pipe JG. Rapid 3D PC-MRA using Spiral Projection Imaging,. ISMRM 2005:2403

Tables

Table 1. Pulse sequence parameters.

	Cartesian	TR-interleaved spiral	Beat-interleaved spiral	Short beat-interleaved spiral
TE/TR	3.4/6.1 ms	3.5/12.0 ms	3.5/16.0 ms	3.5/16.0 ms
Number of interleaves	-	12	9	6
Readout duration	3.0 ms	5.3 ms	9.4 ms	9.3 ms
SENSE factor	2 (Anterior-Posterior)	1	1	1
Segmentation factor	2	1	3	3
Field of view	300x300 mm	260x260 mm	260x260 mm	260x260 mm
Slices	16-18	16-18	16-18	16-18
Voxel size	2.8 mm isotropic	2.8 mm isotropic	2.8 mm isotropic	2.8 mm isotropic
Phase interval	48.8 ms	48.8 ms	48.8 ms	48.8 ms
Flip angle (Ernst angle)	6°	8°	9°	9°
Prescribed scan time	560-644 RR intervals	240-276 RR intervals	240-276 RR intervals	160-184 RR intervals
Navigator gating window	5 mm	5 mm	5 mm	5 mm
Velocity encoding	150 cm/s	150 cm/s	150 cm/s	150 cm/s

Table 2. Actual scan times for all four 4D flow acquisitions.

	Scan times	Relative to Cartesian
Cartesian	14m57s±4m36s	(100 %)
TR interleaved spiral	6m12s±1m16s	43±9 %
Beat interleaved spiral	6m21s±1m32s	44±10 %
Short beat interleaved spiral	4m04s±1m08s	28±5 %

The numbers are given as mean±1SD for n=10.

Table 3. Pathline analysis results.

	Systolic traces within segmentation (%)	Diastolic traces within segmentation (%)
Cartesian	51±16 %	64 ± 6 %
TR interleaved spiral	60±7 %	65 ± 3 %
Beat interleaved spiral	52±10 %	57 ± 5 %
Short beat interleaved spiral	56±11 %	55 ± 6 %

No statistically significant differences were found between any methods for the systolic traces, but the number of diastolic traces within the segmentation for the Cartesian and TR interleaved spiral were significantly higher than for the beat and short beat interleaved spiral methods, using a two-way ANOVA with Tukey post-hoc test for multiple comparisons. The numbers are given as mean±1SD for n=10.

Table 4. Cardiac output analysis results.

	Cardiac output [l/min]	Bias [l/min]	Level of Agreement [l/min]
2D through-plane	6.4±1.6	+0.49	±1.58
Cartesian	6.2± 1.0	+0.26	±0.90
TR interleaved spiral	5.8±1.0	-0.14	±0.69
Beat interleaved spiral	5.7±1.1 *	-0.23	±0.64
Short beat interleaved spiral	5.6±0.8 *	-0.38	±0.73

*: $p<0.05$ versus 2D through-plane using a two-way ANOVA with Tukey post-hoc test for multiple comparisons. No statistically significant differences were found between any of the 3D acquisitions (including both the Cartesian and spiral acquisitions). The numbers are given as mean±1SD for n=10. The bias and level of agreement from the Bland-Altman analysis is also shown for all methods.

Table 5. Background phase errors in-vitro

	Phase error before correction [m/s]	Phase error after correction [m/s]
Cartesian	-0.06±0.02	0.00±0.02
TR interleaved spiral	-0.18±0.03	0.00±0.02
Beat interleaved spiral	-0.16±0.03	0.00±0.02
Short beat interleaved spiral	-0.16±0.03	0.00±0.02

Table 6. In-vitro SNR

	Mean SNR
Cartesian	178±52
TR interleaved spiral	155±51
Beat interleaved spiral	206±70
Short beat interleaved spiral	166±58